Journal of Sea Research 202 (2024) 102540

Contents lists available at ScienceDirect

Journal of Sea Research

journal homepage: www.elsevier.com/locate/seares

Optical distinguishability of phytoplankton species and its implications for hyperspectral remote sensing discrimination potential

Yuan Zhang [a], Fang Shen [a,*], Haiyang Zhao [a], Xuerong Sun [b], Qing Zhu [a], Mengyu Li [a]

[a] State Key Laboratory of Estuarine and Coastal Research, East China Normal University, Shanghai, China
[b] Centre for Geography and Environmental Science, Department of Earth and Environmental Sciences, Faculty of Environment, Science and Economy, University of Exeter, Cornwall, United Kingdom

ARTICLE INFO

Keywords:
Phytoplankton
Optical property
Phytoplankton types discrimination
Hyperspectral remote sensing ;

ABSTRACT

Different phytoplankton types play distinct roles in marine ecosystems, biogeochemical processes, and responses to climate change. Traditionally, phytoplankton classification has heavily relied on chemical analysis methods based on phytoplankton pigments, such as High-Performance Liquid Chromatography (HPLC) analysis. This approach limits the classification resolution to the phylum level of phytoplankton, making it difficult to refine classification to the genus or species level. With the observation of the hyperspectral ocean satellite PACE (Plankton, Aerosol, Cloud, ocean Ecosystem mission) louched by NASA in February 2024, there is potential to achieve finer classification of phytoplankton based on differences in spectral characteristics. This study cultivates various phytoplankton species in the laboratory to observe their light absorption properties (e.g., specific absorption coefficients spectra under unit concentration), investigating the spectral differences between different phyla and among species within the Dinoflagellates and Diatoms. Based on the observed absorption and scattering properties of each phytoplankton species, we simulated the remote sensing reflectance of different species under various ocean color components, examining the potential of hyperspectral remote sensing discrimination of phytoplankton types, and analyzing the impact of Chlorophyll *a* (Chla), colored dissolved organic matter (CDOM), and non-algal particles (NAP) concentrations on the remote sensing discrimination. The results show significant differences in absorption spectra between different groups of phytoplankton (i.e., Diatoms, Dinoflagellates, Xanthophytes, Coccolithophores, Chlorophytes, Cyanobacteria, Cryptophytes). Among species within the Dinoflagellate group, there are also significant spectral differences, while species within the Diatom group exhibit relatively small variations in their spectral shapes. As Chla concentration increases, the potential for remote sensing discrimination of phytoplankton species also increases; conversely, lower Chla concentrations pose greater challenges for remote sensing disscrimiantion. Other ocean color components, such as increased CDOM or NAP concentrations, interfere with the spectral characteristics of phytoplankton in the blue-green spectral domain. Using hierarchical clustering for phytoplankton classification, the results indicate that Cyanobacteria and Chlorophytes can be well distinguished from other group at lower NAP concentrations, while Diatoms, Cryptophytes, and Xanthophytes are not easily distinguishable from each other. Differentiating between species within the same group using remote sensing data presents significant challenges. This study provides a comprehensive investigation into the optical characteristics of different phytoplankton types, laying a foundation for their remote sensing classification and deepening the understanding of the potential of hyperspectral remote sensing for detailed phytoplankton classification.

1. Introduction

Although the biomass of phytoplankton is only 1 % of that of terrestrial plants, it contributes approximately 50 % of global primary productivity (Field et al., 1998; Behrenfeld, 2014). Owing to differences in morphological and physiological characteristics, different phytoplankton play different roles in biogeochemical processes and marine ecosystems (Le Quéré et al., 2005). For example, different diatom species have different cell sizes and cell wall silicon-carbon ratios, resulting in different abilities to transport carbon to the deep sea (Tréguer et al.,

* Corresponding author.
E-mail address: fshen@sklec.ecnu.edu.cn (F. Shen).

https://doi.org/10.1016/j.seares.2024.102540
Received 29 June 2024; Accepted 3 September 2024
Available online 6 September 2024

2018). Approximately 75–80 % of the species of toxic algal bloom species belong to the dinoflagellate group, whereas certain dinoflagellate species do not produce toxins (Janouškovec et al., 2017). Therefore, taxonomic studies of phytoplankton diversity are required to enhance our understanding of phytoplankton function in global biogeochemical cycling processes.

Owing to differences in size, shape, internal and external structure, and pigment composition, different phytoplankton can alter the optical radiation signal (Ciotti et al., 2002; Brewin et al., 2010); therefore, optical radiation-based phytoplankton taxonomy is an important method for current phytoplankton diversity observation studies (Mouw et al., 2017). Optical remote sensing techniques can provide large-scale and long-term measurements of phytoplankton biomass, spatial distribution, taxonomy, and population composition accompanied with the current rapid development of sensor technology. Hyperspectral sensors can provide abundant spectral data for research on biological species of phytoplankton, thereby enhancing their ability to differentiate phytoplankton (Dierssen et al., 2021). Launches of successful hyperspectral satellites, such as GaoFen-5 (Liu et al., 2019), PRISMA (Cogliati et al., 2021), EnMAP (Guanter et al., 2015), and the upcoming PACE mission dedicated to monitoring and investigating phytoplankton species (Werdell et al., 2019), can improve the amount of data available for the remote sensing of phytoplankton species (Dierssen et al., 2020).

Prospective efforts have been made to determine the optical remote sensing potential of various phytoplankton types. For example, Torrecilla et al. (2011) found that remote-sensing reflectance can better identify phytoplankton, and 425–435 and 495–540 nm are the most useful spectral ranges for phytoplankton group research. Xi et al. (2015) used the phytoplankton absorption coefficient, simulated $R_{rs}(\lambda)$, and simulated $R_{rs}(\lambda)$-derived absorption of water compounds to identify the phytoplankton groups. Their results showed that the direct use of the phytoplankton absorption coefficient resulted in excellent phytoplankton, whereas the absorption coefficients derived from the simulated $R_{rs}(\lambda)$ introduced errors, leading to the worst results. Wolanin et al. (2016) applied the absorption coefficients of diatoms, coccolithophores, and cyanobacteria to simulate the $R_{rs}(\lambda)$ under different ocean color conditions. Consequently, through derivative analysis, they explored the band setting of hyperspectral sensors suitable for distinguishing phytoplankton groups. In general, most previous studies are based on in situ or model-simulated absorption or remotely sensed reflectance spectral data, combined with signal processing tools, to analyze the optical properties of phytoplankton, which usually rely on empirical relationships.

To date, studies have rarely focused on the optical properties of phytoplankton species and their hyperspectral characteristics of remote sensing, both in laboratory phytoplankton monoculture settings and in field surveys in natural aquatic environments. Moreover, the use of these hyperspectral characteristics in distinguishing between phytoplankton species, genera, and phyla remains unclear. Recently, a study investigated the absorption properties of phytoplankton groups, and various data analyses (i.e., matrix inversion, derivative analyses, and cluster analysis) were successfully applied to discriminate or quantify the information of eight phytoplankton groups to a certain extent (Sun et al., 2019). However, knowledge and understanding of the optical properties of specific phytoplankton species, particularly their hyperspectral characteristics of remote sensing, is still lacking, which limits subsequent remote sensing applications. Specifically: (i) The absorption characteristics of phytoplankton species remain unclear. More laboratory cultures and measurements are required to examine the optical properties of different phytoplankton species to increase the fundamental understanding of the optical variability of distinct species. (ii) The ability and limitation of using remote sensing reflectance in discriminating phytoplankton species has not been properly investigated, particularly in coastal waters (e.g., those heavily influenced by Colored Dissolved Organic Matter (CDOM) and Non-Algal Particles (NAP)). (iii) At the remote sensing application level, the design of the sensor bandwidth and position setting is reliant on and guided by the optical properties of phytoplankton species. In summary, further research on the optical properties of phytoplankton species is required to expand the understanding of phytoplanktons.

The objectives of this study are as follows: (i) to investigate the absorption properties characteristics through laboratory measurements, analyzing both inter-group and intra-group differences; (ii) to explore the remote sensing identification capability based on phytoplankton species and groups using remote sensing reflectance; (iii) to analyze the impact of CDOM and NAP concentrations on the identification of phytoplankton species; and (iv) to discuss the potential for hyperspectral discrimination phytoplankton types. The results of this study provide a foundation for understanding the feasibility of discriminating phytoplankton using hyperspectral remote sensing.

2. Data and methods

2.1. Laboratory measurements

2.1.1. Phytoplankton species cultures and HPLC pigments

Table 1 lists 14 uni-algal species from seven phytoplankton taxonomic groups cultured in the laboratory. It includes six species in diatoms, three species in dinoflagellates, and one each in xanthophytes, coccolithophores, chlorophytes, cyanobacteria, and cryptophytes groups. *Pseudo-nitzschia pungens*, *Karenia mikimotoi*, *Prorocentrum donghaiense*, *Heterosigma akashiwo*, *Emiliania huxleyi*, *Platymonas subcordiformis* and *Synechococcus* sp. were obtained from Shanghai Guangyu Biological Technology Co, Ltd., and other species from Xiamen University. The algae species were cultured in a light incubator at a temperature of 20 °C under a light dark cycle ratio of 12:12 h and an optical density of 2500 lx.

For each uni-algal species, three different volumes of pure algal liquid were diluted to 1 L with pure seawater, resulting in three samples at different concentrations. Subsequently, each diluted uni-algal sample was simultaneously filtered onto two Whatman GF/F Glass Microfiber filters (0.7 μm, 25 mm) under low vacuum pressure. The filters were stored at −40 °C for further analysis. For each species and concentration, one filter was used to measure the phytoplankton pigment concentration and the other to measure the phytoplankton absorption coefficient ($a_{ph}(\lambda)$).

Phytoplankton pigment concentrations derived from high-performance liquid chromatography (HPLC) were analyzed by the Instrumental Analysis Center of Shanghai Jiao Tong University, using the method proposed by Bidigare et al. (2005). Fourteen phytoplankton pigments were measured, including Fucoxanthin (Fuco) , 19′-but-Fucoxanthin (ButFuco) , 19′-hex-Fucoxanthin (HexFuco) , Diadinoxanthin (Diadino) , Lutein (Lut) , Peridinin (Perid) , Neoxanthin (Neo) , Violaxanthin (Viola) , Zeaxanthin (Zea) , Chl *a* , Chlorophyll *b* (Chl*b*) , Chlorophyll c_1 (Chl c_1) , Chlorophyll c_2 (Chl c_2) , Chlorophyll

Table 1
Information of algae species in the laboratory.

Species Index	Species	Group
A.1	*Skeletonema costatum*	Diatoms
A.2	*Thalassiosira weissflogii*	
A.3	*Chaetoceros debilis*	
A.4	*Chaetoceros curvisetus*	
A.5	*Phaeodactylum tricornutum*	
A.6	*Pseudo-nitzschia pungens*	
B.1	*Karenia mikimotoi*	Dinoflagellates
B.2	*Zooxanthella*	
B.3	*Prorocentrum donghaiense*	
C	*Heterosigma akashiwo*	Xanthophytes
D	*Emiliania huxleyi*	Coccolithophores
E	*Platymonas subcordiformis*	Chlorophytes
F	*Synechococcus* sp.	Cyanobacteria
G	*Cryptomonas* sp.	Cryptophytes

c_3 (Chl c_3). The average value of each pigment from three samples of each algal species was used in this study.

2.1.2. Phytoplankton absorption and backscattering coefficients

The absorption coefficients of total and nonalgal particles, ($a_p(\lambda)$) and ($a_{NAP}(\lambda)$), respectively. Were measured using a PerkinElmer Lambda 1050 UV/VIS spectrophotometer equipped with a 15-cm integrating sphere in the range of 380–720 nm at 2-nm resolution and 1-nm interpolation. Adhering to the NASA and IOCCG ocean optics protocols (Mitchell et al., 2003; Roesler et al., 2018), the $a_p(\lambda)$ and $a_{NAP}(\lambda)$ values were obtained before and after pigment extraction in methanol, respectively. Further, the phytoplankton absorption coefficient ($a_{ph}(\lambda)$) was determined as the difference $a_p(\lambda) - a_{NAP}$. The chlorophyll-specific absorption coefficient ($a^*_{ph}(\lambda)$) was calculated as $a_{ph}(\lambda)$/Chl*a*. To reduce this error, the average value of $a^*_{ph}(\lambda)$ from three samples of each algal species was used in this study.

The attenuation and absorption coefficients of the unialgal species were measured using the spectral absorption and attenuation meter (ac-s, WETLabs Inc.) by pouring diluted samples into the tube. The ac-s meter has 84 bands in the spectrum range of 400–730 nm. Based on the measurement protocol of the ac-s instrument (reference or weblink), the temperature and salinity of the diluted samples were measured for further corrections. The difference between the attenuation and absorption coefficients is the scattering coefficient.

The backscattering coefficients of the uni-algal cultures $b_{b\_ph}(\lambda)$, were measured using the back scattering meter (ECO bb9, WETLabs Inc.). During the measurements, all the lenses of bb9 were completely submerged in the uni-algal water samples in the pure black bucket under dark light conditions, and the volume scattering functions at nine wavebands (i.e., 412, 440, 488, 510, 532, 595, 650, 676, and 715 nm) in the 124° direction were collected. In addition, $b_{b\_ph}(\lambda)$ was further corrected using the corresponding attenuation and absorption coefficients from the ac-s meter coupled with the measured temperature and salinity (Mueller et al. (2002)).

Because of the large volume of uni-algal samples required for measuring the backscattering coefficients, only $b_{b\_ph}(\lambda)$ of *S. costatum*, *T. weissflogii*, *K. mikimotoi*, *E. huxleyi* were collected through bb9. In contrast, those of the remaining 10 species were calculated using the scattering coefficients from the ac-s multiplied by the empirical value of the phytoplankton backscattering scale coefficient of 0.005 (Shen et al., 2019).

2.2. Remote sensing reflectance dataset

In contrast to oceanic waters, which are dominated by phytoplankton, CDOM and NAP also affect $R_{rs}(\lambda)$ in coastal waters. Therefore, using the measured $a^*_{ph}(\lambda)$ and $b_{b\_ph}(\lambda)$ coefficients of the 14 phytoplankton species, the $R_{rs}(\lambda)$ values of different phytoplankton species with different water component compositions were simulated to study the spectral characteristics of $R_{rs}(\lambda)$ in optically complex environments.

According to Gordon et al. (1988) and Lee et al. (2002), $R_{rs}(\lambda)$ can be simulated using the total absorption coefficient ($a(\lambda)$) and total backscattering coefficient($b_b(\lambda)$). The specific calculation process is as follows:

$$R_{rs}(\lambda) = \frac{0.52 \times r_{rs}(\lambda)}{1 - 1.7 \times r_{rs}(\lambda)}\ ,\ \# \tag{1}$$

$$r_{rs}(\lambda) = 0.0895 \times u(\lambda) + 0.1247 \times u(\lambda)^2\ ,\ \# \tag{2}$$

$$u(\lambda) = \frac{b_b(\lambda)}{a(\lambda) + b_b(\lambda)}.\# \tag{3}$$

The total absorption and backscattering coefficients $a(\lambda)$ and $b_b(\lambda)$ can be expressed as the linear sum of the contributions of all ocean color components (Sathyendranath et al., 2001), as follows:

$$a(\lambda) = a_w(\lambda) + a_g(\lambda) + a_{NAP}(\lambda) + a_{ph}(\lambda)\ ,\ \# \tag{4}$$

$$b_b(\lambda) = b_{b\_w}(\lambda) + b_{b\_NAP}(\lambda) + b_{b\_ph}(\lambda)\ ,\ \# \tag{5}$$

where $a_w(\lambda)$ is the absorption coefficient of pure seawater, $a_g(\lambda)$ is the absorption coefficient of the CDOM , $b_{b\_w}(\lambda)$ is the backscattering coefficient of pure seawater, and $b_{b\_NAP}(\lambda)$ is the backscattering coefficient of the NAP. The $a_w(\lambda)$ and $b_{b\_w}(\lambda)$ values were obtained from Pope and Fry (1997) and Morel (1974), respectively. Table 2 lists the calculation formulae for $a_g(\lambda)$, $a_{NAP}(\lambda)$, $a_{ph}(\lambda)$, $b_{b\_NAP}(\lambda)$, and $b_{b\_ph}(\lambda)$.

In the formula for $b_{b\_ph}(\lambda)$ presented in Table 2, λ_0 is the reference wavelength, $b^*_{b\_ph}(\lambda_0)$ is the chlorophyll-specific $b_{b\_ph}(\lambda)$ at the reference wavelength, $b_{b\_ph}(\lambda_0)$ is $b_{b\_ph}(\lambda)$ at reference wavelength, and η is the spectral slope. The backscattering parameters ($b^*_{b\_ph}(\lambda_0)$, η) were obtained by fitting the $b_{b\_ph}(\lambda)$ formula to the measured data.

Because of the strong absorption of water, phytoplankton pigments, and Chl *a* fluorescence, when fitting the backscattering data measured by bb9, the 532 nm wavelength was set as the reference wavelength, and the data at 488, 510, 532, 595, and 650 nm were used for calculation (Whitmire et al., 2010). To fit the backscattering coefficients calculated using the ac-s meter, a reference wavelength of 555 nm was selected. Finally, the mean value of the backscatter parameters for each algal species under the three concentrations was used in this study. Theoretically, η should be positive; that is, the backscattering coefficients should decrease with an increase in wavelength. However, certain values of η derived from the ac-s meter were negative. Under these circumstances, η was set to an empirical value of 1 (Lee et al., 2002). Table 3 lists the retrieved backscattering parameters for each of the algal species.

To eliminate the influence of the value of $R_{rs}(\lambda)$ and only focus on the spectral shape, $R_{rs}(\lambda)$ was normalized as per the process outlined in a previous study (Xi et al., 2015),

$$A = \frac{\int_{\lambda_{min}}^{\lambda_{max}} R_{rs}(\lambda)d\lambda}{\lambda_{max} - \lambda_{min}}\ ,\ \# \tag{7}$$

$$\overline{R_{rs}}(\lambda) = \frac{R_{rs}(\lambda)}{A}\ ,\ \# \tag{8}$$

where $\overline{R_{rs}}(\lambda)$ is the normalized $R_{rs}(\lambda)$, and λ_{min} and λ_{max} represent the minimum and maximum values of the spectral range, respectively. In this study, λ_{min} and λ_{max} were 380 and 720 nm, respectively.

Table 2
Formulae of absorption and backscattering coefficients of water components.

Description	Math Formula	References
Absorption coefficient of CDOM($a_g(\lambda)$)	$a_g(\lambda) = a_g(440)exp(-S_g \times (\lambda - 440))S_g = 0.015$	(Bricaud et al., 1981; Yu, 2013)
Absorption coefficient of NAP ($a_{NAP}(\lambda)$)	$a_{NAP}(\lambda) = a_{NAP}(440)exp(-0.009 \times (\lambda - 440))$ $a_{NAP}(440) = 0.01 \times C_{NAP}$	(Shen et al., 2012)
Absorption coefficient of phytoplankton ($a_{ph}(\lambda)$)	$a_{ph}(\lambda) = a^*_{ph}(\lambda) \times C_{Chl\ a}$	(Devred et al., 2006)
Backscattering coefficient of NAP ($b_{b\_NAP}(\lambda)$)	$b_{b\_NAP}(\lambda) = b_{b\_NAP}(532) \times \left(\frac{532}{\lambda}\right)^n$ $n = 0.4114 \times b_{b\_NAP}(532)^{-0.3}$ $b_{b\_NAP}(532) = 0.0183 \times b_{NAP}(532)$ $b_{NAP}(532) = 0.2 \times C_{NAP}$	(Liu, 2013)
Backscattering coefficient of phytoplankton ($b_{b\_ph}(\lambda)$)	$b_{b\_ph}(\lambda) = b_{b\_ph}(\lambda_0) \times \left(\frac{\lambda_0}{\lambda}\right)^\eta$ $b_{b\_ph}(\lambda_0) = b^*_{b\_ph}(\lambda_0) \times C_{Chl\ a}$	(Werdell et al., 2014)

Table 3
Backscattering parameters of 14 algae species.

Species Index	Species	Reference band (nm)	$b^*_{b\_ph}(\lambda_0)$/ ($m^2 \bullet mg^{-1}$)	η
A.1	*S. costatum*	532	0.00084	1.35
A.2	*T. weissflogii*	532	0.00053	1.60
A.3	*C. debilis*	555	0.00038	0.51
A.4	*C. curvisetus*	555	0.00047	0.13
A.5	*P. tricornutum*	555	0.00227	0.13
A.6	*P. pungens*	555	0.00147	0.64
B.1	*K. mikimotoi*	532	0.00041	0.50
B.2	*Zooxanthella*	555	0.00046	1.00
B.3	*P. donghaiense*	555	0.00068	1.00
C	Xanthophytes	555	0.00009	1.00
D	Coccolithophores	532	0.00104	1.59
E	Chlorophytes	555	0.00018	0.45
F	Cyanobacteria	555	0.00065	3.22
G	Cryptophytes	555	0.00014	1.00

2.3. Divergence index

Derivative analysis can effectively highlight spectral characteristics and has been widely used in spectral studies. The first ($S'(\lambda)$) and second derivatives ($S''(\lambda)$) of the spectra were calculated using the following equations:

$$S'(\lambda) = \frac{S(\lambda+\Delta\lambda) - S(\lambda-\Delta\lambda)}{2\Delta\lambda}, \# \quad (9)$$

$$S''(\lambda) = \frac{S(\lambda+\Delta\lambda) - 2S(\lambda) + S(\lambda-\Delta\lambda)}{(\Delta\lambda)^2}, \# \quad (10)$$

where $\Delta\lambda$ represents the spectral interval between two adjacent bands and $S(\lambda)$ represents the spectra. Because derivative analysis can be easily affected by noise, the measured spectra were smoothed using the Savitzky-Golay filter with a polynomial order and frame length of 4 and 21, respectively.

An $S'(\lambda)$ value of 0 indicates the extremum point (maximum or minimum) of the spectra. Whereas, $S''(\lambda)$ value of 0 indicates the inflection point of the spectra. Thus, setting the sensor band at a higher frequency where the $S'(\lambda)$ and $S''(\lambda)$ are equal to 0 can facilitate the capture of the spectral characteristics (Lee et al., 2007).

To quantify differences between spectra of different phytoplankton groups and species, the divergence index (DI(λ)) was presented in a previous study (Shen et al., 2019),

$$\mathrm{DI}(\lambda) = \frac{1}{\pi} \times arccos\left(\frac{S_1 \bullet S_2}{|S_1| \times |S_2|}\right), \# \quad (11)$$

where S_1 and S_2 represent the two different spectra. The range of DI(λ) varied from 0 to 1. The closer the DI index is to 0, the greater the similarity between the two spectra. In contrast, the closer it is to 1, the greater the difference between the two spectra.

3. Results and discussion

3.1. Difference of phytoplankton absorption property

In this section, the difference of the absorption spectra among various groups is investigated. When analyzing the absorption characteristics and differences among severn phytoplankton groups, *S. costatum* and *K. mikimotoi* were chosen to represent diatoms and dinoflagellates, respectively.

3.1.1. Various phytoplankton groups

To focus on the shape of absorption spectra, the $a^*_{ph}(\lambda)$ was further normalized at 440 nm (i.e., the $a^*_{ph}(\lambda)$ was divided by its $a^*_{ph}(440)$). The normalized $a^*_{ph}(\lambda)$ values of the uni-alagl cultures used in this study are shown in Fig. 1.

Because all the algae species used in this study contained Chl *a*, obvious absorption peaks were observed at approximately 440 and 675 nm in all seven phytoplankton groups (Fig. 1). However, the shapes of the absorption spectra of the seven groups in the other bands were different. The absorption spectra of chlorophytes and cyanobacteria were significantly different from those of other phytoplankton groups. For example, the absorption spectrum of chlorophytes exhibited absorption peak and valley at 480 and 456 nm, respectively. In addition, chlorophytes exhibited a shoulder peak at approximately 650 nm, whereas the remaining phytoplankton groups exhibited an absorption valley. The absorption coefficient of chlorophytes increased with increasing wavelength in the range of 550–675 nm, whereas no such phenomenon was observed in the other phytoplankton groups. The absorption spectra of cyanobacteria exhibited an absorption peak and valley at 490 and 478 nm, respectively, and its absorption spectrum did not change significantly with an increase in wavelength in the range of 570–610 nm. Both the dinoflagellates and coccolithophores exhibited absorption peaks at approximately 465 nm; however, the peak of dinoflagellates was weaker than that of coccolithophores. In addition, it is evident in Fig. 1 that the absorption spectra of diatoms, xanthophytes, and cryptophytes were slightly different.

Table 4 presents the ratio of pigment to Chl *a* concentrations in the seven phytoplankton groups. Chlorophytes were found to be the only group containing the pigments lutein and Chl *b*. Based on the chlorophyll-specific absorption of Chl *b* shown in Fig. 2 (Clementson and Wojtasiewicz, 2019), it can be inferred that the absorption peaks of chlorophytes at 480 and 650 nm were mainly associated with Chl *b*. Further, the differences in the absorption spectra of different phytoplankton groups were owing to the different types and contents of diagnostic pigments of each group (Catlett and Siegel, 2018). In cyanobacteria, only zeaxanthin and diadinoxanthin were detected, and it was the only phytoplankton group that contained zeaxanthin. This indicated that the absorption peak of cyanobacteria at 490 nm was most probably influenced by zeaxanthin, which is consistent with the spectra of zeaxanthin (Fig. 2). Except for 19′-hex-fucoxanthin, dinoflagellates and coccolithophores shared the same type of pigment (Table 4). For example, only two groups contained Chl c_3. According to the spectra of Chl c_3 shown in Fig. 2, the absorption peak of dinoflagellates and coccolithophores at approximately 465 nm was most probably owing to the absorption by Chl c_3. Moreover, because the ratio of Chl c_3 to Chl *a* of coccolithophores Was higher than that of dinoflagellates, the absorption peak of coccolithophores was more obvious at approximately 465 nm. Xanthophytes and cryptophytes contained the same type of pigment, which may explain why the absorption spectra of xanthophytes and cryptophytes were similar. Except for violaxanthin, diatoms, xanthophytes, and cryptophytes have the same type of pigment.

To quantitatively analyze the differences between the absorption spectra of different phytoplankton groups, the DI(λ) values of the absorption spectra of the seven phytoplankton groups were calculated, as shown in Fig. 3. It was found that the DI(λ) between the absorption spectra of any two phytoplankton groups was less than 0.1 in the ranges of 400–430 and 680–720 nm. Whereas, large differences were mainly observed in the range of 430–680 nm. The DI(λ) of the absorption spectra of any two groups of diatoms, xanthophytes, and cryptophytes were less than 0.2 for the entire wavelengths, except for that in the range of 570–585 nm. In contrast, the DI(λ) between diatoms and the remaining phytoplankton groups (except xanthophytes and cryptophytes) was greater than 0.5, in the range of 400–500 nm. In particular, the DI(λ) between diatoms and coccolithophores, chlorophytes, and cyanobacteria were approximately 1, indicating that the existence of large differences in the spectra between diatoms and the three groups. Except in the ranges of 455–458 and 566–589 nm, the DI(λ) values between diatoms and dinoflagellates were less than 0.4.

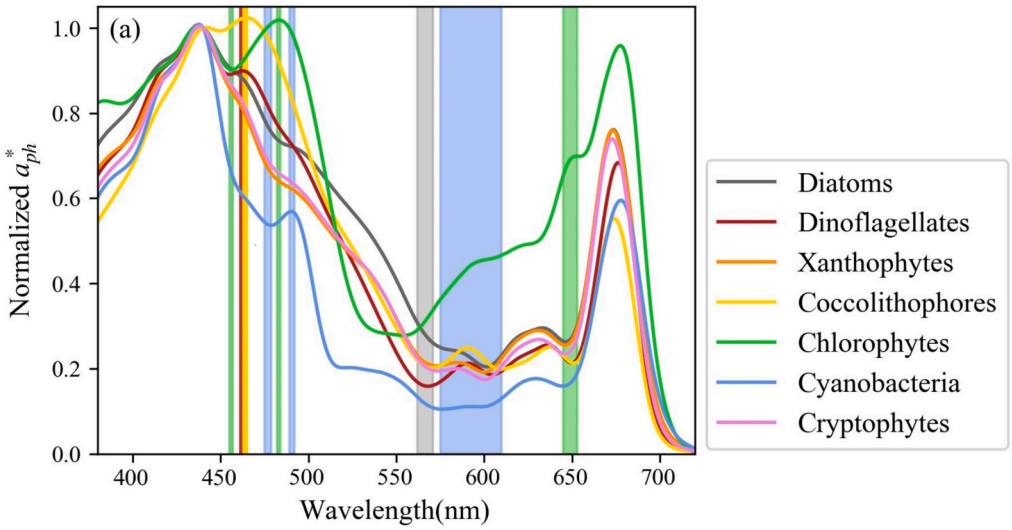

Fig. 1. Normalized $a^*_{ph}(\lambda)$of seven phytoplankton groups. The red, gold, green, and blue shadows in (a) represent the spectral ranges where the absorption spectrum of dinoflagellates, chrysophytes, chlorophytes, and cyanobacteria exhibit considerable differences compared with other phytoplankton groups, respectively. (For interpretation of the references to color in this figure legend, the reader is referred to the web version of this article.)

Table 4
Ratio of pigment concentration to Chl *a* concentration in seven phytoplankton groups.

Group	Chl c_3	Chl c_2	Chl c_1	ButFuco	Fuco	Neo	Viola	HexFuco	Diadino	Zea	Lut	Chl *b*
Dinoflagellates	0.01	0.09	–	0.02	0.14	0.01	–	0.06	0.07	–	–	–
Coccolithophores	0.20	0.24	–	–	0.28	0.32	–	0.22	0.15	–	–	–
Diatoms	–	0.34	0.02	–	0.70	–	–	–	0.11	–	–	–
Cyanobacteria	–	–	–	–		–	–	–	0.01	0.19	–	–
Xanthophytes	–	0.06	0.03	–	0.31	–	0.06	–	0.03	–	–	–
Chlorophytes	–	–	–	–	0.03	0.07	0.06	–	–	–	0.06	0.62
Cryptophytes	–	0.07	0.03	–	0.37	–	0.06	–	0.04	–	–	–

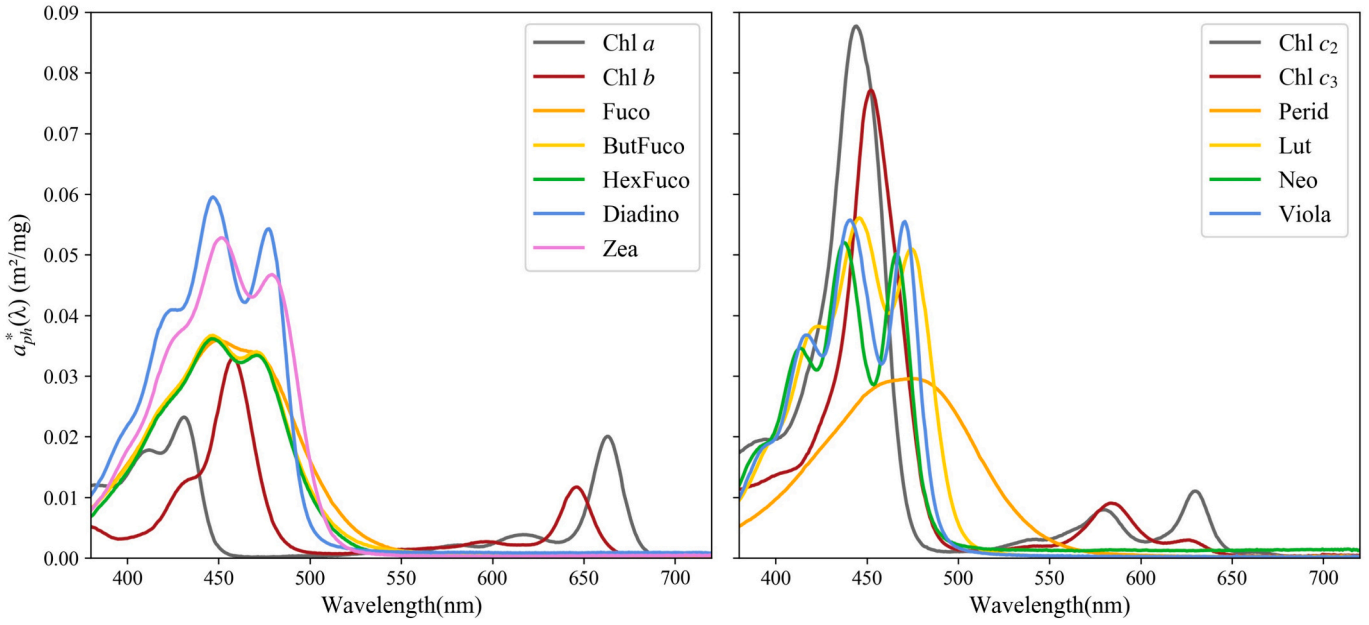

Fig. 2. Chlorophyll-specific absorption spectra of phytoplankton pigments from (Clementson and Wojtasiewicz, 2019).

When comparing the dinoflagellates and other groups, the DI(λ) values between the absorption spectra dinoflagellates and that of xanthophytes (Fig. 3f), coccolithophores and cryptophytes (Fig. 3m) were less than 0.65 in the entire spectral range. Consider the coccolithophores as an example. Except that the DI(λ) between dinoflagellate and coccolithophores (Fig. 3g), coccolithophores and chlorophytes (Fig. 3n) were approximately 0.6 at 455 nm, that between the coccolithophores and the other groups were approximately 1, indicating the existence of

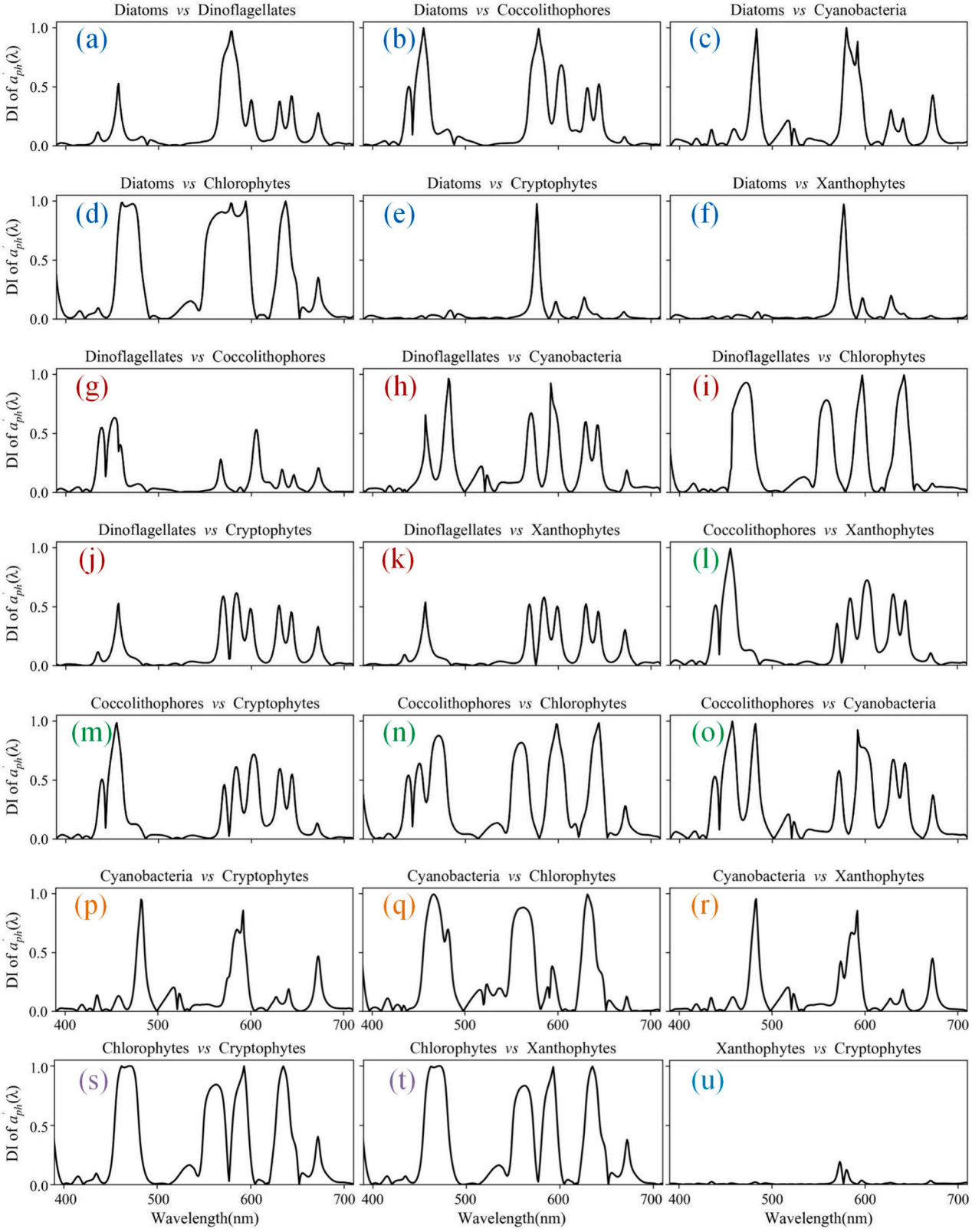

Fig. 3. Divergence index of absorption spectra among seven phytoplankton groups.

significant differences. Similarly, large differences in DI(λ) values were observed between cyanobacteria and the other groups. For example, the value of DI(λ) between the cyanobacteria and chlorophytes was approximately 0.7 at 480 nm, whereas those between cyanobacteria and the other phytoplankton groups reached 1. In the ranges of 465–476 and 635–640 nm, the DI(λ) between the absorption spectra of chlorophytes and the other phytoplankton groups was greater than 0.5. Further, that between the absorption spectra of xanthophytes and cryptophytes was less than 0.2 in the entire spectral range. In addition, the DI(λ) values between the absorption spectra of xanthophytes and the other

phytoplankton groups were the same as those between the cryptophytes and other phytoplankton groups.

3.1.2. Various diatoms species

The $a^*_{ph}(\lambda)$ values for the six diatom species are shown in Fig. 4. The shapes of the absorption spectra of the six diatoms were similar, with only slight differences. For example, in the range of 475–500 nm, *S. costatum*, *T. weissflogii,* and *P. tricornutum* exhibited shoulder peaks. Whereas, in the range of 575–600 nm, with the exception of *S. costatum*, the other five diatom species exhibited small absorption peaks.

Fig. 5 shows that the absorption spectra of *S. costatum* and other diatoms had DI(λ) values of approximately 1 at 577 nm, indicating the high potential of this alga for optical differentiation. Nonetheless, with the exception of *S. costatum*, the DI(λ) values between the absorption spectra of the two diatoms were less than 0.5 across the entire spectral range. Particularly, the DI(λ) values between the absorption spectra of *C. debilis, C. curvisetus*, and *P. tricornutum* were less than 0.25 across the entire spectral range, thereby indicating the poor capacity of these algae in differentiating among one another.

Moreover, the difference in absorption spectra between xanthophytes and certain diatom species was less than that between the two diatoms species. For example, the DI(λ) value between the absorption spectra of *T. weissflogii* and xanthophytes was smaller than that between *T. weissflogii* and *P. pungens*. Furthermore, the absorption spectra of *T. weissflogii* and xanthophytes were more similar to each other than those of *T. weissflogii* and *P. pungens*.

As shown in Table 5, the six diatom species contain the same four pigment types; however, the ratio between the concentration of the phytoplankton pigments and Chl *a* concentration was different.

3.1.3. Various dinoflagellate species

Fig. 6 depicts the $a^*_{ph}(\lambda)$ spectra of the three methanogenic species. The absorption spectrum of *K. mikimotoi* differed significantly from those of *Zooxanthella* and *P. donghaiense*. All three species contained an extra absorption peak near 465 nm, with *K. mikimotoi* exhibiting the smallest absorption peak. *K. mikimotoi* displayed a pronounced absorption valley at approximately 650 nm, whereas *Zooxanthella* and *P. donghaiense* lacked this characteristic.

Within the three dinoflagellate species, differences were smaller between *Zooxanthella* and *P. donghaiense*, with DI(λ) values lower than 0.45 in the full spectral range (Fig. 7). This similarity results in similar DI values between *Zooxanthella*, *P. donghaiense,* and other phytoplankton groups. Large differences were observed between *K. mikimotoi* and the other two dinoflagellate species, where the DI(λ) value reached 1 at 640 nm. In the range of 440–480 nm, except for the small DI(λ) between the absorption spectra of *Zooxanthella* (or *P. donghaiense*) and coccolithophores, the DI(λ) between the absorption spectra of *Zooxanthella* and other phytoplankton groups was close to 1. In the 620–650 nm spectral range, with the exception of chlorophytes, the DI value between the absorption spectra of *Zooxanthella* and other phytoplankton groups was close to 1, whereas that between the absorption spectra of *K. mikimotoi* and chlorophytes was close to 1 in this spectral range. In addition, the DI (λ) between the absorption spectra of *K. mikimotoi* and other phytoplankton groups was less than 0.5.

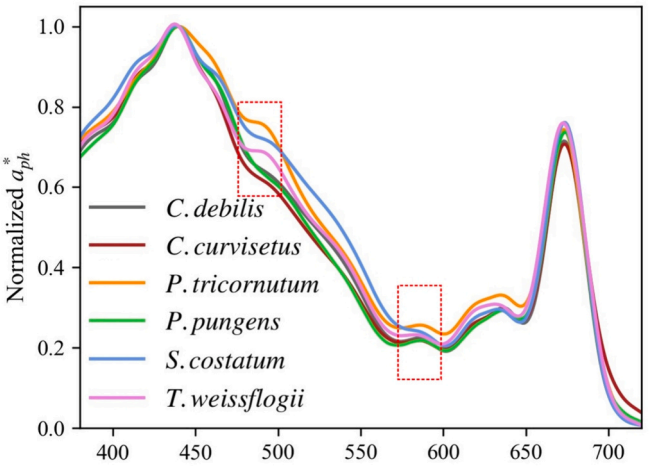

Fig. 4. Normalized $a^*_{ph}(\lambda)$ of six diatom species.

Different types of pigments in the three dinoflagellate species may be the primary reason for differences in their absorption spectra (Table 6). In general, peridinin is a diagnostic pigment for dinoflagellates and fucoxanthin is a diagnostic pigment for diatoms (Vidussi et al., 2001). However, as a dinoflagellate, *K. mikimotoi* does not contain peridinin and rather contains fucoxanthin. In addition, compared with *Zooxanthella* and *P. donghaiense*, *K. mikimotoi* also contains 19′-hex-fucoxanthin, Chl c_3, and neoxanthin, which are found in other groups such as diatoms.

According to Table 6 and Fig. 7, the additional absorption peaks of *Zooxanthella* and *P. donghaiense* at approximately 465 nm were mainly caused by peridinin. Although *K. mikimotoi* does not contain peridinin, the presence of Chl c_3 may be the reason for the absorption peak at approximately 465 nm. In addition, the absorption spectra of the three dinoflagellate species at 550–650 nm were significantly different, which may be due to the different types of Chl *c*.

3.2. Differnece of phytoplankton R_{rs}

We further analyzed the changes in optical properties under different biomass conditions, as shown in Fig. 8. To highlight the spectral characteristics, the first derivative of normalized $R_{rs}(\lambda)$ ($R'_{rs}(\lambda)$) was calculated. Fig. 8 shows that different phytoplankton groups at NAP concentrations are 0 g/m^3, $a_g(440)$ is 0 m^{-1}, $R'_{rs}(\lambda)$ spectrum changes with Chl *a* concentration. It is evident that when Chl *a* concentration is 0.1 mg/m^3, the $R'_{rs}(\lambda)$ of different phytoplankton groups the performance were consistent, which is greater than 0 before 410 nm, less than 0 after 410 nm, and close to 0 after 520 nm. Thus, the original $R_{rs}(\lambda)$ first increases with the increase in wavelength, then decreased with the increase in wavelength after 410 nm, and finally became constant. With an increase in Chl *a* concentration, the $R'_{rs}(\lambda)$ of different phytoplankton groups showed differences. However, above 610 nm, the $R'_{rs}(\lambda)$ remained close to 0. This was mainly owing to the strong absorption of water in the red band, resulting in the spectral characteristics of the phytoplankton contribution being covered. (See Figs. 9 and 10.)

It was found that $R'_{rs}(\lambda)$ of cyanobacteria was quite different from that of other phytoplankton groups. The $R'_{rs}(\lambda)$ of cyanobacteria was greater than 0 in the range–440-460 nm. At approximately 440 and 460 nm, the original $R_{rs}(\lambda)$ of cyanobacteria had an extreme point. In the range of 450–500 nm, the $R'_{rs}(\lambda)$ of chlorophytes is different from that of other phytoplankton groups. It was found from the absorption spectrum of chlorophytes that the reason for this phenomenon may be the absorption peak at approximately 480 nm.

$R'_{rs}(\lambda)$ of diatoms under the four conditions of Chl *a* concentration in the 580–675 nm spectral range is the lowest among the seven phytoplankton groups, and a valley was formed at approximately 655 nm. In Fig. 8, with an increase in Chl *a* concentration, the $R'_{rs}(\lambda)$ of diatoms formed a peak at approximately 685 nm and passed through 0 at 675 and 695 nm, indicating that the original $R_{rs}(\lambda)$ exhibited an extreme point. With the continuous increase in Chl *a* concentration, the $R'_{rs}(\lambda)$ of other phytoplankton groups also formed a peak at approximately 685 nm, with extreme points at 675 and 695 nm. Combined with the absorption spectrum analysis, it was found that the characteristics of $R_{rs}(\lambda)$ in the range of 650–700 nm were mainly caused by Chl *a*. Because the $a^*_{ph}(\lambda)$ of diatoms was higher, the remote sensing characteristics in this spectral range were observed when the Chl *a* concentration in diatoms was low.

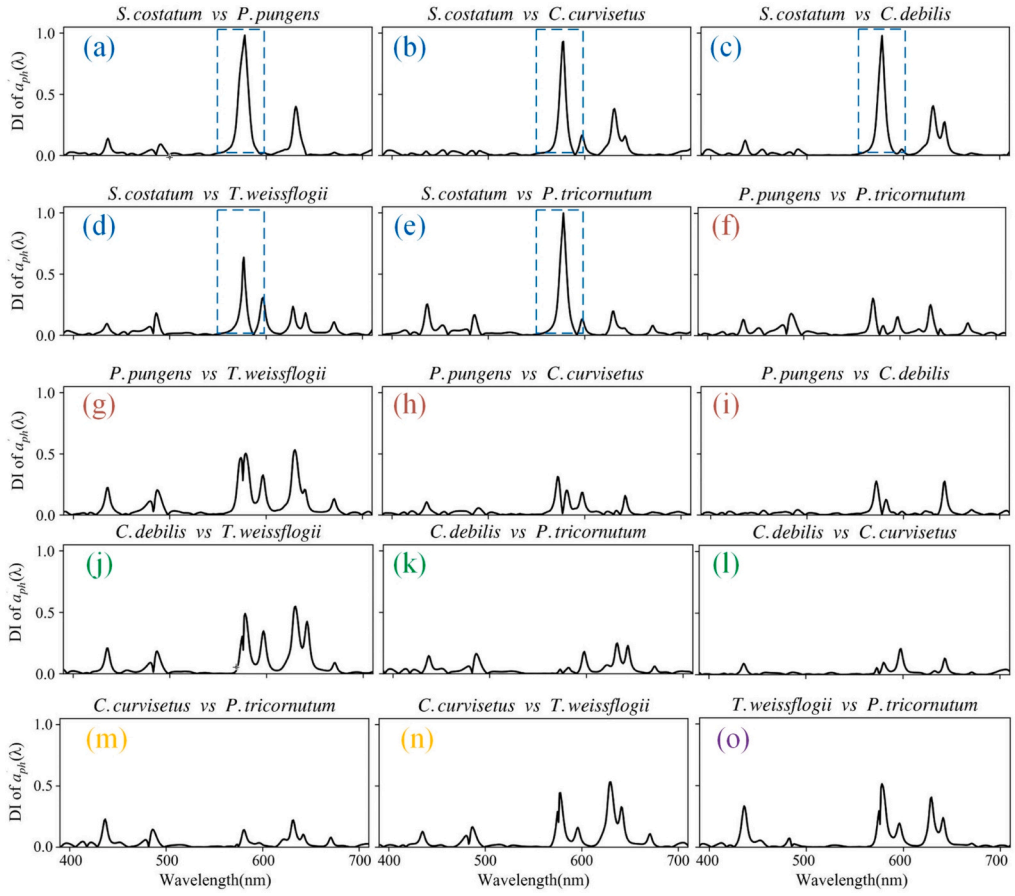

Fig. 5. Divergence index of absorption spectra amongsix diatom species.

Table 5
Phytoplankton pigments and the ratio of pigment concentration to Chl *a* concentration in six diatom species.

Species Name	Chl c_2	Chl c_1	Fuco	Diadino
S. costatum	0.32	0.02	0.70	0.11
P. pungens	0.13	0.04	0.60	0.09
C. curvisetus	0.05	0.09	0.40	0.11
P. tricornutum	0.11	0.25	0.72	0.25
T. weissflogii	0.04	0.03	0.42	0.15
C. debilis	0.06	0.06	0.44	0.09

3.3. Impact of CDOM and NAP

In coastal waters, R_{rs} is influenced by various water color components and their concentrations. Therefore, we investigated the effects of different concentrations of CDOM and NAP on the optical properties of phytoplankton. We explored $R_{rs}(\lambda)$ under two scenarios, specifically: (1) CDOM cannot be ignored, whereas NAP was ignored. The specific values were: Chl *a* concentration is 2.5 mg/m^3 , $a_g(440)$ is 0.075–0.5 m^{-1}, NAP concentration 0.1 g/m^3; (2) Neither CDOM nor NAP can be ignored. The specific values were: Chl *a* concentration is 2.5 mg/m^3, $a_g(440)$ is 0.1 m^{-1}, NAP concentration is 1–50 g/m^3.

Fig. 9 shows the different phytoplankton groups at NAP concentration was 0 g/m^3 and Chl *a* concentration was 2.5 mg/m^3, the $R'_{rs}(\lambda)$ spectrum changed with different $a_g(440)$. With increase in the $a_g(440)$, the characteristics of $R'_{rs}(\lambda)$ before 550 nm gradually disappeared. When $a_g(440)$ was 0.5 m^{-1}, the $R'_{rs}(\lambda)$ of different phytoplankton groups was greater and lesser than 0 within the range of lesser and greater than 570 nm. Thus, the original $R_{rs}(\lambda)$ increased and decreased with the increase in wavelength when less and greater than 570 nm, respectively. Further,

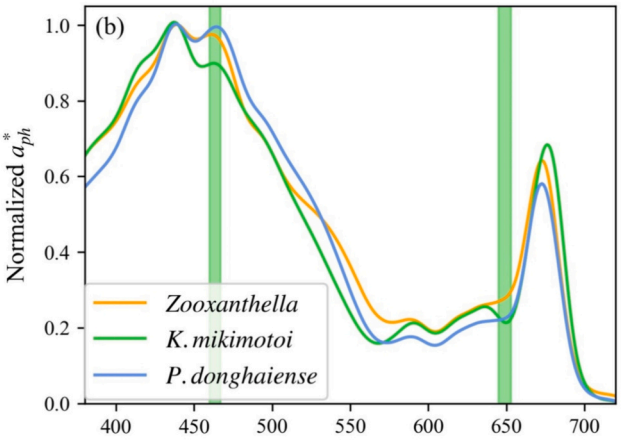

Fig. 6. Normalized $a^*_{ph}(\lambda)$ of three dinoflagellate species. The orange and green shadows in (b) represent the spectral ranges where the absorption spectrum of Zooxanthella and K. mikimotoi have great differences compared with other dinoflagellate species, respectively. (For interpretation of the references to color in this figure legend, the reader is referred to the web version of this article.)

it was found that when $a_g(440)$ was 0.5 m^{-1}, the $R'_{rs}(\lambda)$ of cyanobacteria was still different from the other phytoplankton groups at approximately 450 and 500 nm.

The $R'_{rs}(\lambda)$ of different phytoplankton groups in the range of 550–610 nm exhibited large fluctuations (first decreased rapidly and then increased rapidly). This can be primarily attributed to the absorption coefficient of water significantly changes within the spectral

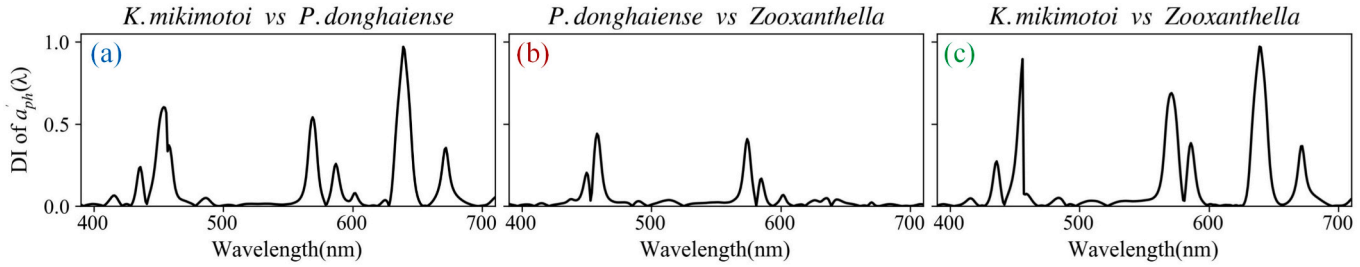

Fig. 7. Divergence index of absorption spectra between three dinoflagellate species.

Table 6
Phytoplankton pigments and the ratio of pigment concentration to Chl a concentration in three dinoflagellate species.

Species Name	Chl c_3	Chl c_2	Chl c_1	Perid	ButFuco	Fuco	Neo	HexFuco	Diadino
K. mikimotoi	0.10	0.09	–	–	0.02	0.14	0.10	0.06	0.07
P. donghaiense	–	0.21	–	0.99	0.09	–	–	–	0.11
Zooxanthella sp.	–	0.41	0.02	0.87	0.06	–	–	–	0.20

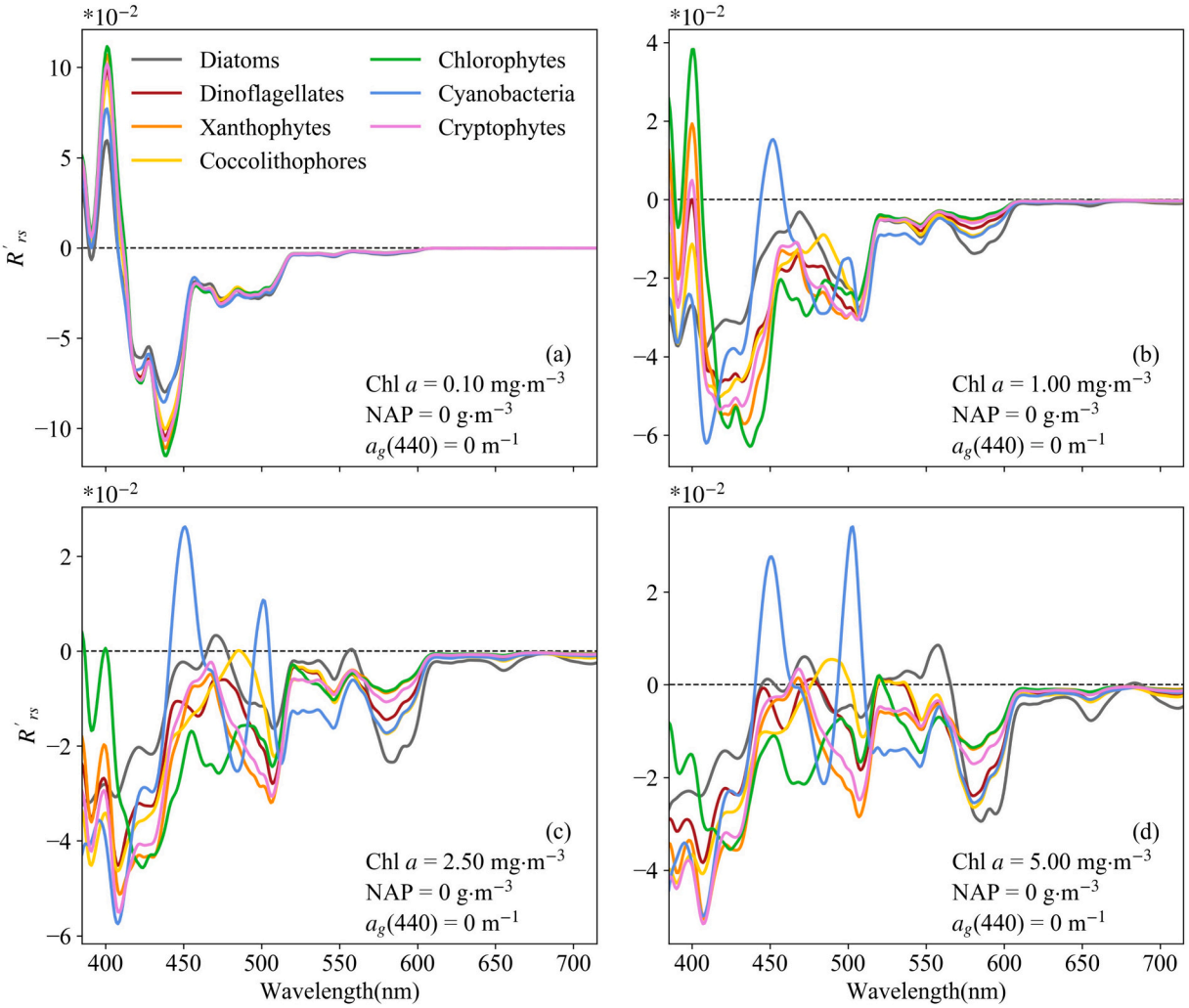

Fig. 8. When the NAP concentration is 0 g/m^3 and $a_g(440)$ is 0 m^{-1}, the $R_{rs}^{'}(\lambda)$ of different phytoplankton groups changes with the Chl *a* concentration, where (a) - (d) represent that the Chl *a* concentration is 0.10 mg/m^3, 1 mg/m^3, 2.5 mg/m^3 and 5 mg/m^3 respectively.

range.

Fig. 10 shows that the $R_{rs}^{'}(\lambda)$ changes with NAP concentrations with Chl *a* concentration of 2.5 mg/m^3 and $a_g(440)$ of 0.1 m^{-1}. Similar to the effect of CDOM, with the increase in NAP concentration, the $R_{rs}^{'}(\lambda)$ characteristics of different phytoplankton groups gradually disappeared before 550 nm. When the NAP concentration was 50 g/m^3, the $R_{rs}^{'}(\lambda)$ of

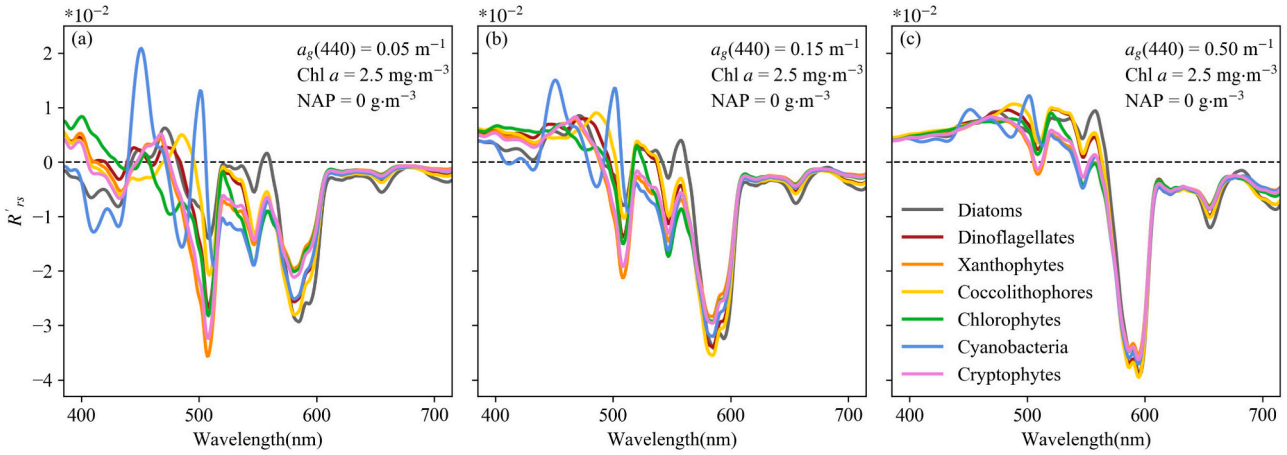

Fig. 9. When the NAP concentration is 0 g/m^3 and the Chl *a* concentration is 2.5 mg/m^3, the $R'_{rs}(\lambda)$ of different phytoplankton groups changes with the $a_g(440)$, where (a) - (c) represent $a_g(440)$ is 0.05m^{-1}, 0.15m^{-1}, 0.5m^{-1} (respectively).

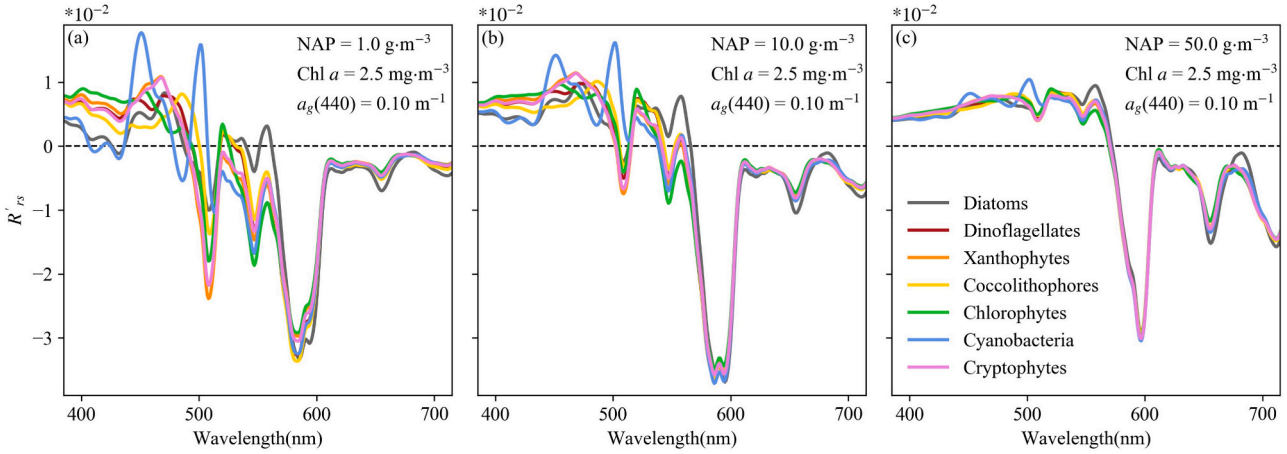

Fig. 10. When the Chl *a* concentration is 2.5 mg/m^3 and $a_g(440)$ is 0.1m^{-1}, the $R'_{rs}(\lambda)$ of different phytoplankton groups changes with the NAP concentration, where (a) - (c) represent the NAP concentration is 1g/m^3, 10 g/m^3 and 50 g/m^3 (respectively).

cyanobacteria could still be distinguished from other phytoplankton groups at approximately 450 and 500 nm.

In general, with an increase in CDOM or NAP concentration, the $R_{rs}(\lambda)$ spectral characteristics contributed by phytoplankton in the short-wavelength position gradually disappeared. This was primarily because the absorption of CDOM and NAP decreased with increasing wavelength, thus exhibiting strong absorption under blue light. Although the backscattering of NAP also decreased with increasing wavelength, the absorption of NAP was much greater than the backscattering in the blue light range.

3.4. Potential of hyperspectral remote sensing

PACE (NASA's Plankton, Aerosol, Cloud, ocean Ecosystem mission) is the first global hyperspectral mission for ocean and atmospheric observation, equipped with a hyperspectral imager called OCI. OCI features continuous hyperspectral capabilities from ultraviolet to near-infrared, with a nominal spectral step size of 2.5 nm and an average bandwidth of approximately 5 nm, covering a spectral range of 340–890 nm. The spatial resolution of OCI imagery is about 1 km^2 at its lowest point, with a swath width of 2663 km, enabling global coverage every two days. To explore its potential for monitoring phytoplankton diversity, we used the HCA method to further analyze the possibility of hyperspectral resolution of phytoplankton under three different scenarios, as shown in Fig. 11.

Fig. 11 (a) shows scenario A, wherein the phytoplankton was dominant, CDOM and NAP were ignored. The cyanobacteria and chlorophytes could be well distinguished from other group, mainly because the absorption spectra of cyanobacteria and chlorophytes were quite different from other phytoplankton groups. In addition, coccolithophores could also be well distinguished from the other phytoplankton groups. It was difficult to distinguish between *T. weissflogii*, *C. debilis*, xanthophytes, and cryptophytes mainly because the absorption spectra of diatoms, xanthophytes, and cryptophytes are similar. Dinoflagellates can also be distinguished from other phytoplankton groups; however, distinguishing between the three dinoflagellate species was challenging.

Fig. 11(b) shows scenario B, wherein CDOM was not ignored while NAP was. Cyanobacteria could still be effectively distinguished from the other phytoplankton groups, whereas chlorophytes could be distinguished from the other phytoplankton groups under most conditions. However, a misclassification with other phytoplankton groups occurred. Dinoflagellates could be distinguished from the other phytoplankton groups under most conditions; however, they were misclassified as diatoms and coccolithophores.

Fig. 11 (c) shows the results of HCA based on $R_{rs}(\lambda)$ in scenario C wherein both CDOM and NAP were not ignored. With the increase in NAP concentration, except for cyanobacteria, which could be

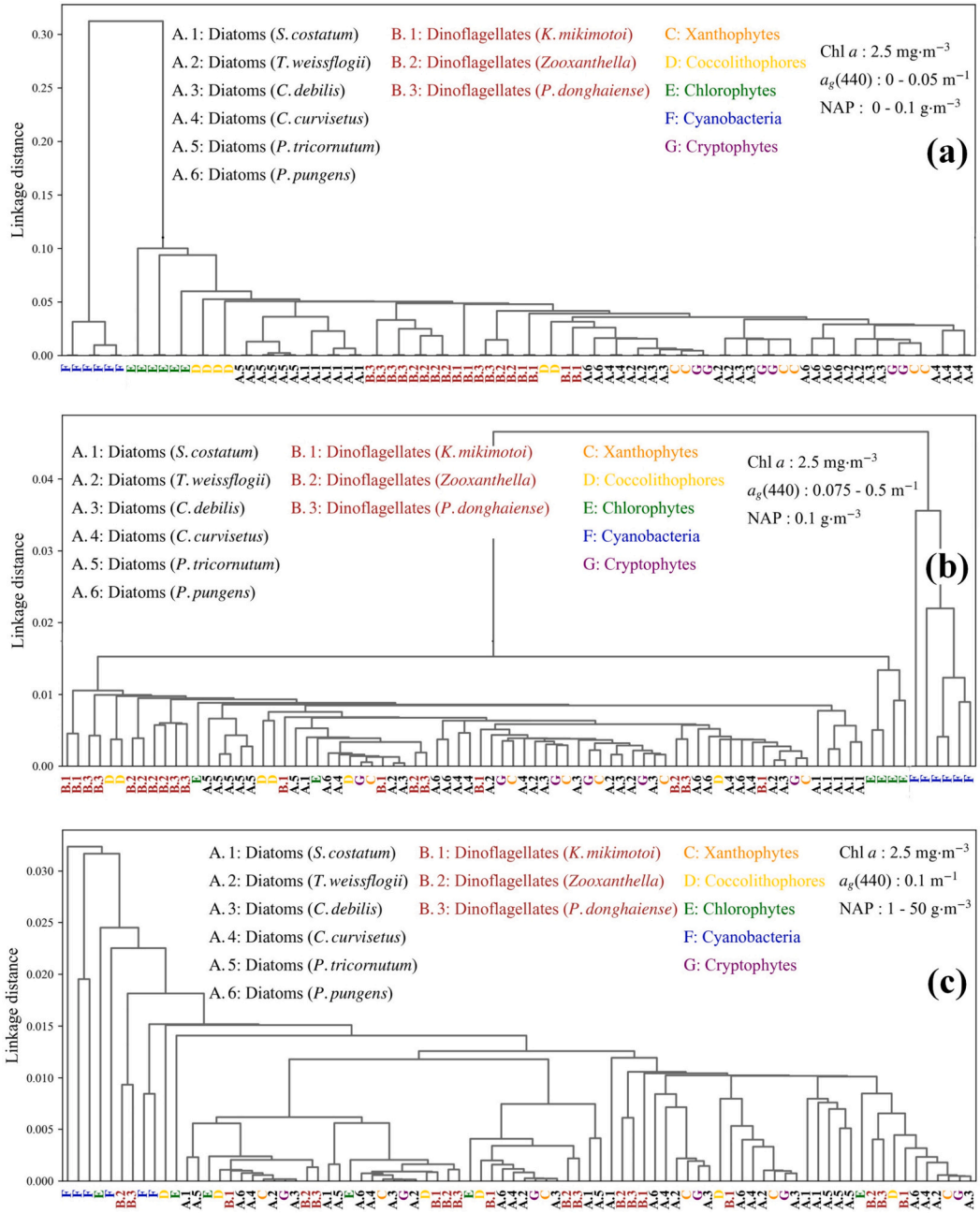

Fig. 11. The results of HCA based on three scenarios.

distinguished from the other phytoplankton groups under certain conditions, the distinguishability between different phytoplankton groups decrease. The HCA was not suitable for the remote sensing distinguishing of phytoplankton species in this scenario, and a new method must be developed.

In general, when phytoplankton biomass is high or the NAP concentration is low, phytoplankton can be distinguished based on $R_{rs}(\lambda)$. When the NAP concentration is high, that is, in turbid coastal waters, the effect of identifying phytoplankton groups based on $R_{rs}(\lambda)$ is reduced. The mean absolute percentage error of Zhu et al. (2019) established that the phytoplankton species composition model increases by 17 % with increase in the NAP concentration from 0 to 200 g/m^3. Cyanobacteria and chlorophytes are easy to identify compared with other phytoplankton groups, and can be well distinguished from other phytoplankton group under the condition of high NAP concentration, Xi et al. (2017) reached the same conclusion. From Fig. 11, it was found that the linkage distance between diatoms, xanthophyta, and cryptophytes was small, and remote sensing discrimination encounters considerable challenges.

4. Conclusion

By capturing continuous and detailed spectral information, hyperspectral technology is gradually becoming a forefront hotspot in phytoplankton remote sensing research. This study investigates the optical properties of different phytoplankton types and their potential for discrimination using hyperspectral remote sensing through laboratory measurements and remote sensing reflectance simulations. The main conclusions are as follows:

(1) There were significant differences in the absorption spectra of different groups, particularly in case of cyanobacteria and

chlorophytes. This is mainly because of the different types of phytoplankton pigments contained in different phytoplankton groups. Among the three dinoflagellates, the absorption spectra of *K. mikimotoi* were quite different from those of other dinoflagellate species, mainly because of the large differences in the types of phytoplankton pigments contained in different dinoflagellates. The absorption coefficient spectra of the six diatom species were similar because they contained the same phytoplankton pigments. Moreover, the difference in the absorption spectra between xanthophyta and some diatoms was less than that between diatoms.

(2) With an increase in Chl *a* concentration, the difference in $R_{rs}(\lambda)$ of different phytoplankton groups increased. When Chl *a* concentration was low, distinguishing phytoplankton groups based on $R_{rs}(\lambda)$ was challenging.

(3) As the concentrations of colored dissolved organic matter or non-algal particles increase, the remote sensing spectral features contributed by phytoplankton in the short-wavelength region become progressively obscured. This presents a challenge for distinguishing phytoplankton species using remote sensing reflectance under such conditions.

(4) The HCA results based on $R_{rs}(\lambda)$ showed that when phytoplankton were dominant, with the exception of diatoms, cryptoalgae, and xanthophyta, different groups could be effectively distinguished by $R_{rs}(\lambda)$. Cyanobacteria and chlorophytes were the easiest algae species to be identified based on $R_{rs}(\lambda)$. However, remote-sensing discrimination between different species in the same phytoplankton group remains a challenging task.

This study explores the optical properties of phytoplankton and analyzes the potential of using hyperspectral technology to distinguish different phytoplankton types. It provides an important basis for the development of hyperspectral remote sensing methods for phytoplankton diversity inversion.

CRediT authorship contribution statement

Yuan Zhang: Formal analysis, Investigation, Writing – review & editing. **Fang Shen:** Conceptualization, Funding acquisition. **Haiyang Zhao:** Methodology, Software, Visualization, Writing – original draft. **Xuerong Sun:** Writing – review & editing. **Qing Zhu:** Data curation, Writing – review & editing. **Mengyu Li:** Data curation, Methodology, Writing – review & editing.

Declaration of competing interest

The authors declare that they have no known competing financial interests or personal relationships that could have appeared to influence the work reported in this paper.

Data availability

Data will be made available on request.

Acknowledgments

This study was funded by the National Natural Science Foundation of China [Grant No. 42076187 and No.42271348].

References

Behrenfeld, M.J., 2014. Climate-mediated dance of the plankton. Nat. Clim. Chang. 4, 880–887.
Bidigare, R.R., Van Heukelem, L., Trees, C.C., 2005. In: Andersen, R.A. (Ed.), Analysis of Algal Pigments by High- Performance Liquid Chromatography[M]. Algal Culturing Techniques. Elsevier Academic Press, pp. 327–345.
Brewin, R.J.W., Lavender, S.J., Hardman-Mountford, N.J., Hirata, T., 2010. A spectral response approach for detecting dominant phytoplankton size class from satellite remote sensing. Acta Oceanol. Sin. 29, 14–32.
Bricaud, A., Morel, A., Prieur, L., 1981. Absorption by dissolved organic matter of the sea (yellow substance) in the UV and visible domains. Limnol. Oceanogr. 26, 43–53.
Catlett, D., Siegel, D.A., 2018. Phytoplankton pigment communities can be modeled using unique relationships with spectral absorption signatures in a dynamic coastal environment. J. Geophys. Res. Oceans 123, 246–264.
Ciotti, Á.M., Lewis, M.R., Cullen, J.J., 2002. Assessment of the relationships between dominant cell size in natural phytoplankton communities and the spectral shape of the absorption coefficient. Limnol. Oceanogr. 47, 404–417.
Clementson, L.A., Wojtasiewicz, B., 2019. Dataset on the absorption characteristics of extracted phytoplankton pigments. Data Brief 24, 103875.
Cogliati, S., Sarti, F., Chiarantini, L., Cosi, M., Lorusso, R., Lopinto, E., Miglietta, F., Genesio, L., Guanter, L., Damm, A., Pérez-López, S., Scheffler, D., Tagliabue, G., Panigada, C., Rascher, U., Dowling, T.P.F., Giardino, C., Colombo, R., 2021. The PRISMA imaging spectroscopy mission: overview and first performance analysis. Remote Sens. Environ. 262, 112499.
Devred, E., Sathyendranath, S., Stuart, V., Maass, H., Ulloa, O., Platt, T., 2006. A two-component model of phytoplankton absorption in the open ocean: theory and applications. J. Geophys. Res. Oceans 111.
Dierssen, H., Bracher, A., Brando, V., Loisel, H., Ruddick, K., 2020. Data needs for hyperspectral detection of algal diversity across the globe. Oceanography 33, 74–79.
Dierssen, H.M., Ackleson, S.G., Joyce, K.E., Hestir, E.L., Castagna, A., Lavender, S., McManus, M.A., 2021. Living up to the hype of hyperspectral aquatic remote sensing: science, resources and outlook. Front. Environ. Sci. 9.
Field, C.B., Behrenfeld, M.J., Randerson, J.T., Falkowski, P., 1998. Primary production of the biosphere: integrating terrestrial and oceanic components. Science 281, 237–240.
Gordon, H.R., Brown, O.B., Evans, R.H., Brown, J.W., Smith, R.C., 1988. A semianalytic radiance model of ocean color. J. Geophys. Res. Atmos. 93, 10909–10924.
Guanter, L., Kaufmann, H., Segl, K., Foerster, S., Rogass, C., Chabrillat, S., Kuester, T., Hollstein, A., Rossner, G., Chlebek, C., Straif, C., Fischer, S., Schrader, S., Storch, T., Heiden, U., Mueller, A., Bachmann, M., Mühle, H., Müller, R., Habermeyer, M., Ohndorf, A., Hill, J., Buddenbaum, H., Hostert, P., van der Linden, S., Leitão, P., Rabe, A., Doerffer, R., Krasemann, H., Xi, H., Mauser, W., Hank, T., Locherer, M., Rast, M., Staenz, K., Sang, B., 2015. The EnMAP spaceborne imaging spectroscopy mission for earth observation. Remote Sens. 7, 8830–8857.
Janouškovec, J., Gavelis, G.S., Burki, F., Dinh, D., Bachvaroff, T.R., Gornik, S.G., Bright, K.J., Imanian, B., Strom, S.L., Delwiche, C.F., Waller, R.F., Fensome, R.A., Leander, B.S., Rohwer, F.L., Saldarriaga, J.F., 2017. Major transitions in dinoflagellate evolution unveiled by phylotranscriptomics. Proc. Natl. Acad. Sci. 114, E171–E180.
Le Quéré, C., Harrison, S.P., Prentice, I.C., Buitenhuis, E.T., Aumont, O., Bopp, L., Claustre, H., Cunha, L.C.D., Geider, R., Giraud, X., Klaas, C., Kohfeld, K.E., Legendre, L., Manizza, M., Platt, T., Rivkin, R.B., Sathyendranath, S., Uitz, J., Watson, A.J., Wolf-Gladrow, D., 2005. Ecosystem dynamics based on plankton functional types for global ocean biogeochemistry models. Glob. Chang. Biol. 11, 2016–2040.
Lee, Z., Carder, K.L., Arnone, R.A., 2002. Deriving inherent optical properties from water color: a multiband quasi-analytical algorithm for optically deep waters. Appl. Opt. 41, 5755–5772.
Lee, Z., Carder, K., Arnone, R., He, M., 2007. Determination of primary spectral bands for remote sensing of aquatic environments. Sensors 7, 3428–3441.
Liu, M., 2013. Scattering Properties of Suspended Particles in High Turbid Waters and Remote Sensing Application. Master Thesis. East China Normal University, Shanghai, China.
Liu, Y., Zhang, J., Zhang, Y., Sun, W., Jiao, L., Sun, D., Hu, X., Ye, X., Li, Y., Liu, S., Cao, K., Chai, M., Zhou, W., 2019. The advanced hyperspectral imager: aboard China's GaoFen-5 satellite. IEEE Geosci. Remote Sens. Mag. 7, 23–32.
Mitchell, B.G., Kahru, M., Wieland, J., Stramska, M., 2003. Determination of spectral absorption coefficients of parti- cles, dissolved material and phytoplankton for discrete water samples. In: Mueller, J.L., Fargion, G.S., McClain, C.R. (Eds.), Ocean Optics Protocols for Satellite Ocean Color Sensor Validation, Revision 4, Volume Iv: Inherent Optical Properties: Instruments, Characterizations, Field Measurements and Data Analysis Protocols. National Aeronautical and Space Administration.
Morel, A., 1974. Optical properties of pure water and pure sea water. In: Jerlov, N.G., Nielsen, E.S. (Eds.), Optical Aspects of Oceanography, New York. Academic Press.
Mouw, C.B., Hardman-Mountford, N.J., Alvain, S., Bracher, A., Brewin, R.J.W., Bricaud, A., Ciotti, A.M., Devred, E., Fujiwara, A., Hirata, T., Hirawake, T., Kostadinov, T.S., Roy, S., Uitz, J., 2017. A consumer's guide to satellite remote sensing of multiple phytoplankton groups in the global ocean. Front. Mar. Sci. 4, 41.
Mueller, J.L., Fargion, G.S., McClain, C.R., 2002. Ocean Optics Protocols for Satellite Ocean Color Sensor Validation, Revision 4, Volume IV: Inherent Optical Properties: Instruments, Characterizations, Field Measurements and Data Analysis Protocols. Goddard Space Flight Space Center.
Pope, R.M., Fry, E.S., 1997. Absorption spectrum (380-700 nm) of pure water. II. Integrating cavity measurements. Appl. Opt. 36, 8710–8723.
Roesler, C., Stramski, D., Sa, E.J.D., Röttgers, R., Reynolds, R.A., 2018. Chapter 5: Spectrophotometric measure- ments of particulate absorption using filter pads. In: Neeley, A.R., Mannino, A. (Eds.), Ocean Optics & Biogeochemistry Protocols for Satellite Ocean Colour Sensor Validation, Volume 1: Inherent Optical Property Measurements and Protocols: Absorption Coefficient (v1.0). International Ocean Colour Coordinating Group (IOCCG) in Collaboration With National Aeronautics and Space Administration (NASA).

Sathyendranath, S., Cota, G., Stuart, V., Maass, H., Platt, T., 2001. Remote sensing of phytoplankton pigments: a comparison of empirical and theoretical approaches. Int. J. Remote Sens. 22, 249–273.
Shen, F., Zhou, Y., Hong, G., 2012. Absorption property of non-algal particles and contribution to total light absorption in optically complex waters, a case study in Yangtze and adjacent coast. In: International Conference on Environment Science, pp. 61–66. Melbourne, Australia.
Shen, F., Tang, R., Sun, X., Liu, D., 2019. Simple methods for satellite identification of algal blooms and species using 10-year time series data from the East China Sea. Remote Sens. Environ. 235, 111484.
Sun, X.R., Shen, F., Brewin, R.J.W., Liu, D.Y., Tang, R.G., 2019. Twenty-year variations in satellite-derived chlorophyll-a and phytoplankton size in the Bohai Sea and Yellow Sea. J. Geophys. Res. Oceans 124, 8887–8912.
Torrecilla, E., Stramski, D., Reynolds, R.A., Millán-Núñez, E., Piera, J., 2011. Cluster analysis of hyperspectral optical data for discriminating phytoplankton pigment assemblages in the open ocean. Remote Sens. Environ. 115, 2578–2593.
Tréguer, P., Bowler, C., Moriceau, B., Dutkiewicz, S., Gehlen, M., Aumont, O., Bittner, L., Dugdale, R., Finkel, Z., Iudicone, D., Jahn, O., Guidi, L., Lasbleiz, M., Leblanc, K., Levy, M., Pondaven, P., 2018. Influence of diatom diversity on the ocean biological carbon pump. Nat. Geosci. 11, 27–37.
Vidussi, F., Claustre, H., Manca, B.B., Luchetta, A., Marty, J.C., 2001. Phytoplankton pigment distribution in relation to upper thermocline circulation in the eastern Mediterranean Sea during winter. J. Geophys. Res. Oceans 106, 19939–19956.
Werdell, P.J., Roesler, C.S., Goes, J.I., 2014. Discrimination of phytoplankton functional groups using an ocean reflectance inversion model. Appl. Opt. 53, 4833–4849.
Werdell, P.J., Behrenfeld, M.J., Bontempi, P.S., Boss, E., Cairns, B., Davis, G.T., Franz, B. A., Gliese, U.B., Gorman, E.T., Hasekamp, O., Knobelspiesse, K.D., Mannino, A., Martins, J.V., McClain, C.R., Meister, G., Remer, L.A., 2019. The plankton, aerosol, cloud, ocean ecosystem mission: status, Science, advances. Bull. Am. Meteorol. Soc. 100, 1775–1794.
Whitmire, A.L., Pegau, W.S., Karp-Boss, L., Boss, E., Cowles, T.J., 2010. Spectral backscattering properties of marine phytoplankton cultures. Opt. Express 18, 15073–15093.
Wolanin, A., Soppa, M., Bracher, A., 2016. Investigation of spectral band requirements for improving retrievals of phytoplankton functional types. Remote Sens. 8, 871.
Xi, H., Hieronymi, M., Röttgers, R., Krasemann, H., Qiu, Z., 2015. Hyperspectral differentiation of phytoplankton taxonomic groups: a comparison between using remote sensing reflectance and absorption spectra. Remote Sens. 7, 14781–14805.
Xi, H., Hieronymi, M., Krasemann, H., Röttgers, R., 2017. Phytoplankton group identification using simulated and in situ hyperspectral remote sensing reflectance. Front. Mar. Sci. 4, 272.
Yu, X., 2013. Measurements of Pigment Absorption Coefficients and Retrieval Models of Pigment Concentration in Turbid Coastal Waters. Master Thesis. East China Normal University, Shanghai, China.
Zhu, Q., Shen, F., Shang, P., Pan, Y., Li, M., 2019. Hyperspectral remote sensing of phytoplankton species composition based on transfer learning. Remote Sens. 11, 2001.